Supplementary Information for "Excess area dependent scaling behavior of nano-sized membrane tethers"

N. Ramakrishnan[1], K. K. Sreeja[2], Arpita Roychoudhury[3], David M. Eckmann[1,4], Portonovo S. Ayyaswamy[5], Tobias Baumgart[6], Thomas Pucadyil[7], Shivprasad Patil[3], Valerie M. Weaver[8], Ravi Radhakrishnan[1,2,9,*]

[1]Department of Bioengineering, University of Pennsylvania, Philadelphia, PA, 19104, USA,
[2]Department of Chemical and Biomolecular engineering, University of Pennsylvania, Philadelphia, PA, 19104, USA,
[3]Department of Physics, Indian Institute of Science Education and Research, Pune, 411008, India,
[4]Department of Anesthesiology and Critical Care, University of Pennsylvania, Philadelphia, PA, 19104, USA,
[5]Department of Mechanical engineering and Applied Mechanics, University of Pennsylvania, Philadelphia, PA, 19104, USA,
[6]Department of Chemistry, University of Pennsylvania, Philadelphia, PA, 19104, USA,
[7]Department of Biology, Indian Institute of Science Education and Research, Pune, 411008, India,
[8]Department of Surgery and Anatomy, University of California San Francisco, San Francisco, CA, 94143, USA,
[9]Department of Biochemistry and Biophysics, University of Pennsylvania, Philadelphia, PA, 19104, USA

E-mail: * rradhak@seas.upenn.edu

Contents

S1. Dynamical Triangulated Monte Carlo

The dynamical triangulation Monte Carlo technique consists of two independent moves to alter the degrees of freedom that define the triangulated surface which is taken as a model for the fluid membrane [1–3]:

(a) **Vertex Move:** A randomly chosen vertex is randomly displaced to a new position within a cube of size ϵ, centered around the vertex. The move is performed by the holding the connectivity fixed as shown in Fig. S1(a) and accepted using the Metropolis scheme [4]. This move is only performed in both the constant N-σ-τ-T and N-σ-$\mathcal{A}_{\rm patch}$-T ensembles.

(b) **Link Flip:** A randomly chosen tether shared between two triangles on the surface is removed and reconnected between the two previously unconnected vertices as shown in Fig. S1(b), by holding the vertex positions fixed. This move is only performed in both the constant N-σ-τ-T and N-σ-$\mathcal{A}_{\rm patch}$-T ensembles.

(c) **Boundary Move:** In this move, the x and y dimensions of the membrane patch is randomly changed from $L_x \rightarrow L_x^{'}$ and $L_y \rightarrow L_y^{'}$ which results in a change in membrane the projected area from $\mathcal{A}_{\rm patch} \rightarrow \mathcal{A}_{\rm patch}{}^{'}$. Unlike moves (i) and (ii), which only alters local conformational states, the boundary move is designed to alter the global conformations of the membrane patch. This move is only performed in the constant N-σ-τ-T ensemble.

All the three moves are accepted using the standard Metropolis scheme with a probability given by the Boltzmann constant of the energy change ($\Delta\mathcal{H}_{\rm tot}$) due to the move. In the case of tether pulling simulations the total energy of the membrane is given by $\mathcal{H}_{\rm tot} = \mathcal{H} + \mathcal{H}_{\rm bias}$, where $\mathcal{H}$ denotes the elastic Hamiltonian and $\mathcal{H}_{\rm bias}$ is the harmonic biasing potential as defined in the main manuscript. Here, $k_{\rm B}T = 1$ is the inverse temperature, with $k_{\rm B}$ the Boltzmann constant and T the absolute temperature.

The state of the membrane can be affected by variations either in the bending stiffness or in the self-avoidance parameter, leading to membranes with different excess areas $\mathcal{A}_{\rm ex}$. Snapshots of the membrane conformations in the parameter space of bending rigidity and excess area are shown in Fig. S3.

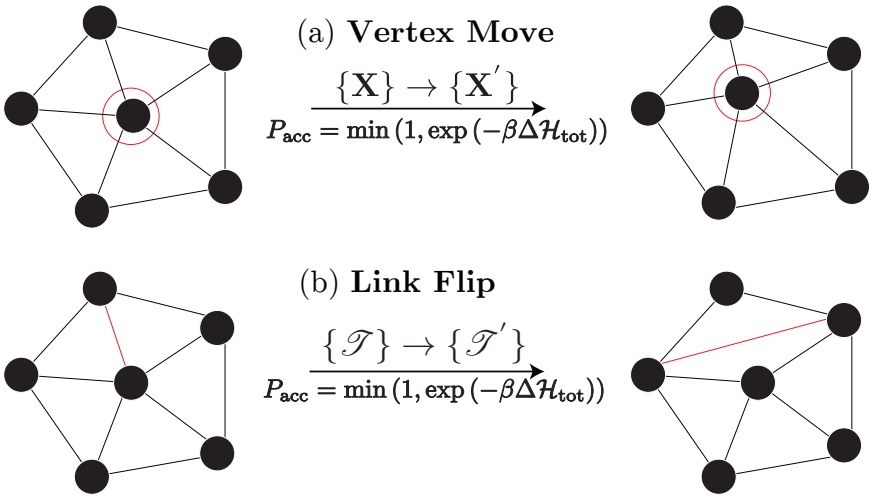

Figure S1. Dynamical triangulated Monte Carlo scheme to independently modify the position (a) and the connectivity (b) of the vertices in the triangulated surface model.

S2. Mapping between membrane frame tension τ and excess area $\mathcal{A}_{\rm ex}$

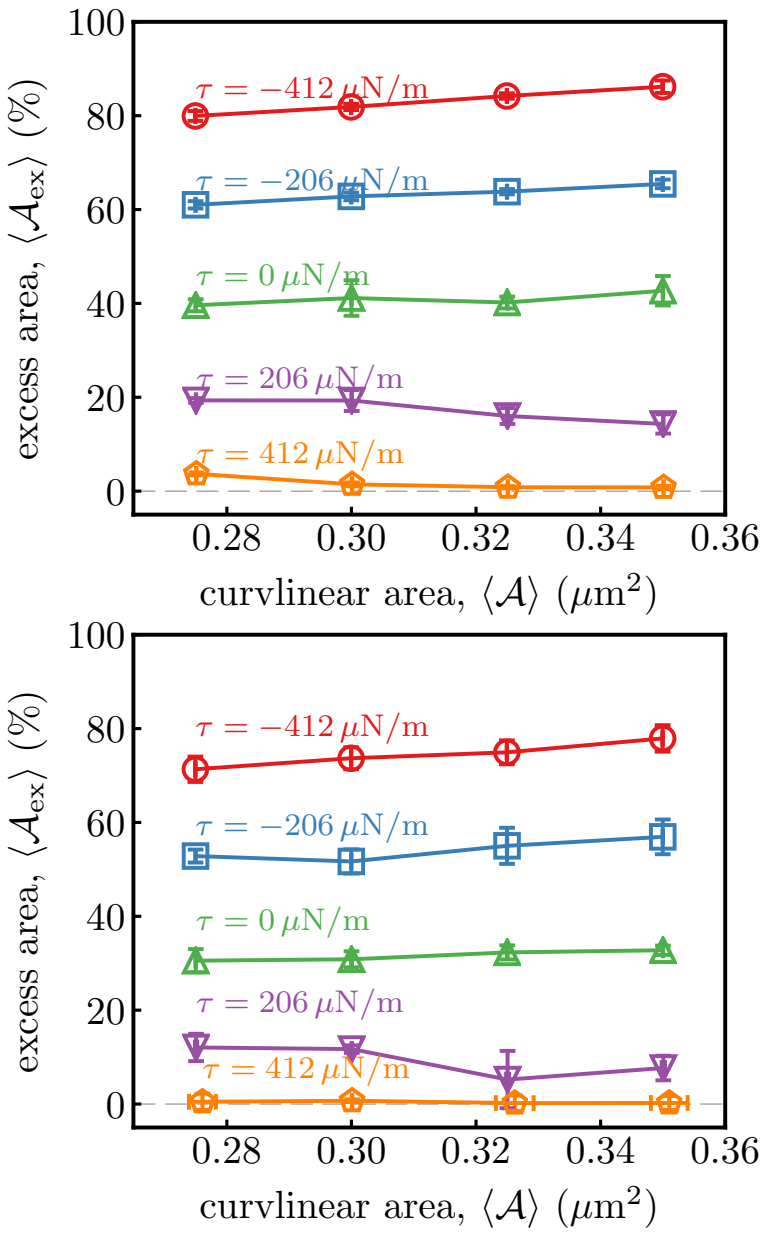

Figure S2. Excess area as a function of the frame tension for membrane patches with $\kappa = 40$ (top) and 160 $k_{\rm B}T$ (bottom). Data shown for five different values of $\tau = -412,\ -206,\ 0,\ 206$ and $412\ \mu$N/m .

S3. Membrane conformations in various limits

The conformations of a planar membrane, when $\mathcal{H}_{\rm bias} = 0$, for two different bending rigidities ($\kappa = 10$ and $40\ k_{\rm B}T$) for two different values of $\mathcal{A}_{\rm ex}$ ($= 4\%$ and 40%) are shown in Fig. S3. The surface is colored with respect to the z position of the vertices.

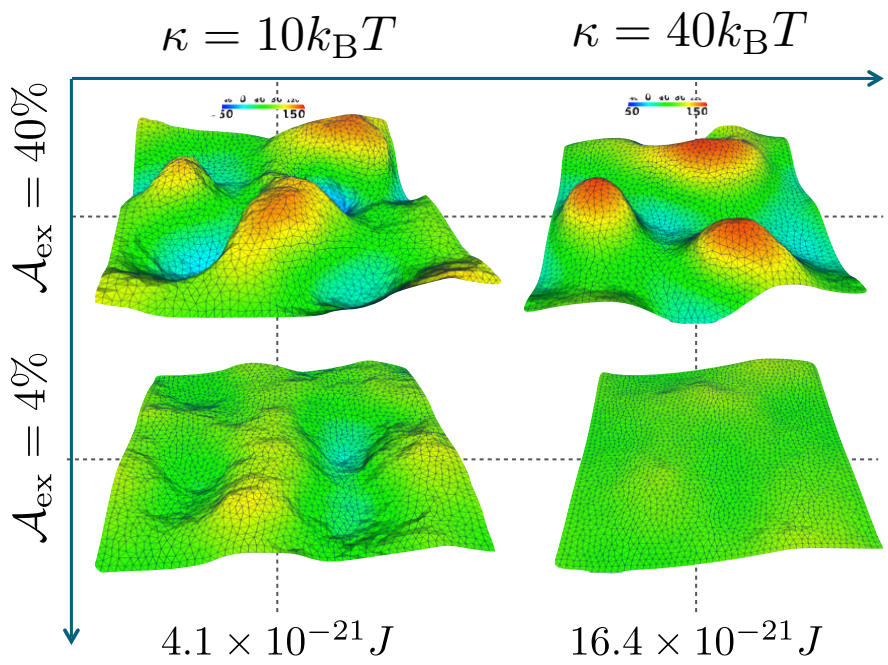

Figure S3. Conformations of membranes with different bending stiffness and excess area. Shown are shapes for two values of the excess area $\mathcal{A}_{\rm ex} = 4$ and 40%.

S4. Undulation spectrum for the planar membrane

In the continuum limit, a planar membrane can be parameterized based on its height with respect to a reference plane and such a parameterization is called the Monge gauge. If the reference plane is taken to be the plane, then the height of the membrane at a chosen point on the plane, with coordinates x and y, is given by $h(x, y)$. The height of the membrane can also be expressed in terms of its Fourier modes as [5]

$$h(\mathbf{X}) = \frac{1}{\mathcal{L}^2_{\text{patch}}} \int d\mathbf{q}\; h_{\mathbf{q}} \exp(-i\mathbf{q}\cdot\mathbf{X}) \tag{S1}$$

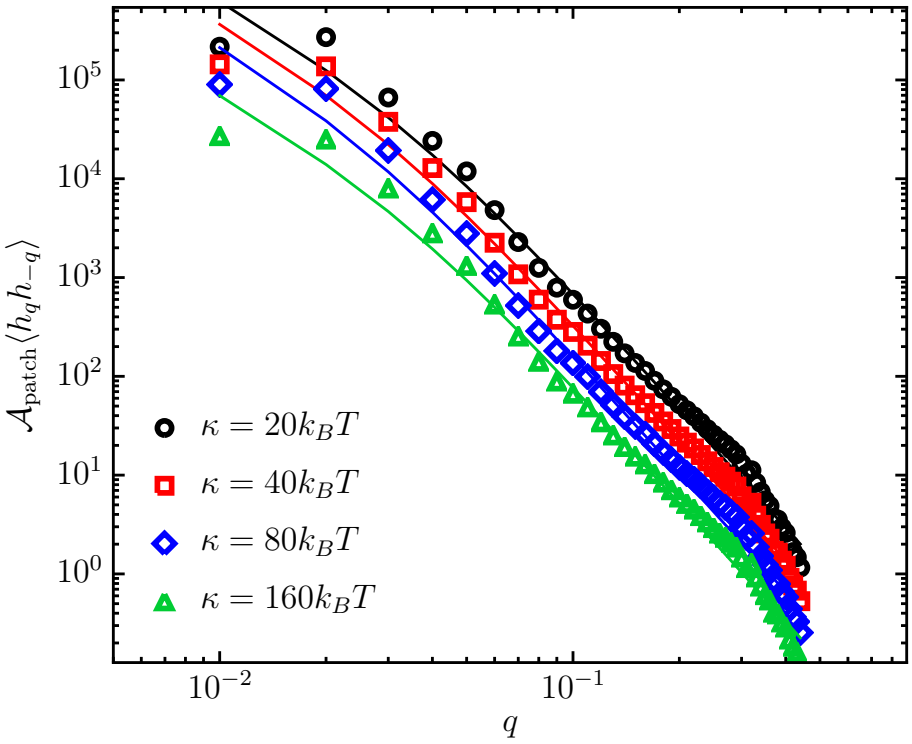

Figure S4. Validation of the small deformation limit. The power spectrum, for each of the Fourier modes, scales as q^{-4} when the membranes have small excess area or large bending stiffness.

Here we have used the short hand notations $\mathbf{X} = [x, y]$ and $\mathbf{q} = [q_x, q_y]$ to denote two dimensional real and Fourier spaces and the Fourier amplitude also has two components given by $h_{\mathbf{q}} = [h_{q_x}, h_{q_y}]$. When the elastic Hamiltonian $\mathcal{H}$ (see eqn. 1 of the main manuscript) is expressed in terms of its Fourier modes, the power spectrum for each of the modes can be shown to obey the relation,

$$\mathcal{A}_{\text{patch}}\,\langle h_q h_{-q}\rangle = \frac{k_{\text{B}}T}{\kappa q^4 + \sigma q^2} \tag{S2}$$

This result is derived for nearly planar membranes (where $|\nabla h \ll 1|$) and hence should be reproducible in the simulations for membranes with either large bending stiffnesses or small excess areas or both. The power spectrum for planar membranes with small excess

area and for a range of values of is shown in Fig. S4. The observed undulation modes scale as q^{-4}, which is in good agreement with the theoretical expression given above. However, it should be remembered that membranes with large excess area would not adhere to this scaling behavior, since the excess area manifests as large amplitude undulations, which takes the systems beyond the small deformation limit (as $|\nabla h \sim 1|$).

S5. Defining the reaction coordinate for tether extraction assays

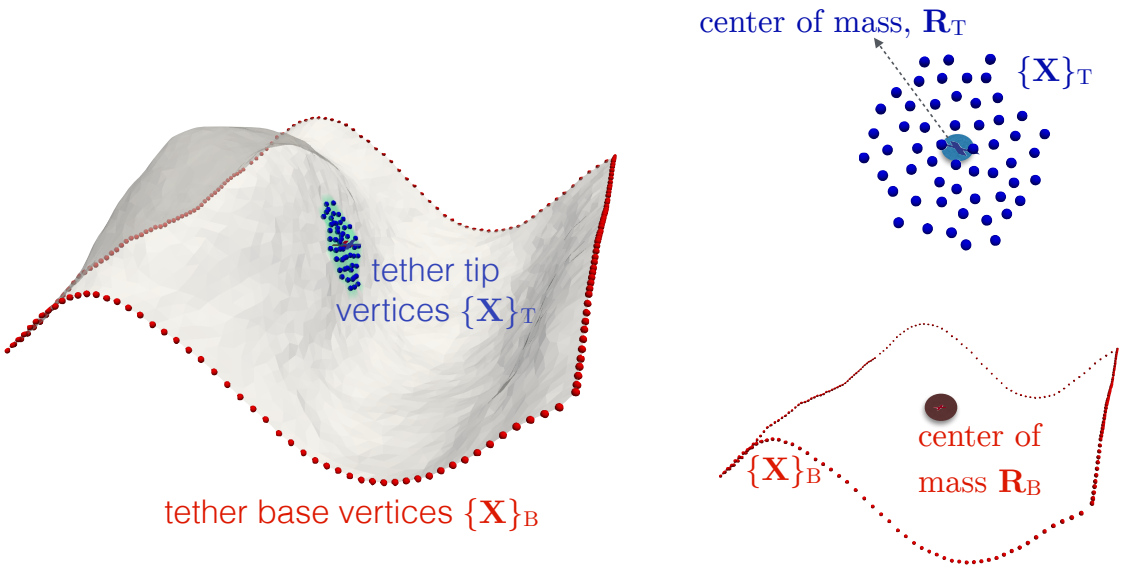

Figure S5. Illustration of the various variables that are used to define the reaction coordinate for tether extraction.

As is shown in the main manuscript, we use the length of the tether l_t as the reaction coordinate for tether extraction and extract tether through a umbrella sampling technique. In our calculations, l_t is defined based on the various variables shown in Fig. S5. The base of the tether is given by $\mathbf{R}_\mathrm{B}$, the center of mass of all vertices on the boundary on the membrane patch — these vertices are denoted $\mathbf{X}_\mathrm{B}$ in Fig. S5. Similarly the position of the tip is given by $\mathbf{R}_\mathrm{T}$ which corresponds to the center of mass of a set of selected vertices denoted $\mathbf{X}_\mathrm{T}$ in Fig. S5. The vertices that constitute $\mathbf{X}_\mathrm{T}$ are selected such that their size is equal to $\mathcal{R}_\mathrm{bead}$, the radius of the bead used for tether extraction. The instantaneous tether length is computed in our calculations as l_t=$|\mathbf{R}_\mathrm{T}-\mathbf{R}_\mathrm{B}|$.

S6. Properties of the tether as a function of κ and $\mathcal{A}_{\rm ex}$

In this section, we display the effect of the membrane excess area and bending rigidity on the length and radius of a tether extracted from a cell membrane. In Fig. S6 we show $l_{\rm t}$ and $\mathcal{R}_{\rm t}$, along with the membrane conformations, as a function of the imposed tether length $\mathcal{L}_{\rm t}$ for a membrane with $\kappa = 20\,k_{\rm B}T$ and $\mathcal{A}_{\rm ex} \sim 10\%$.

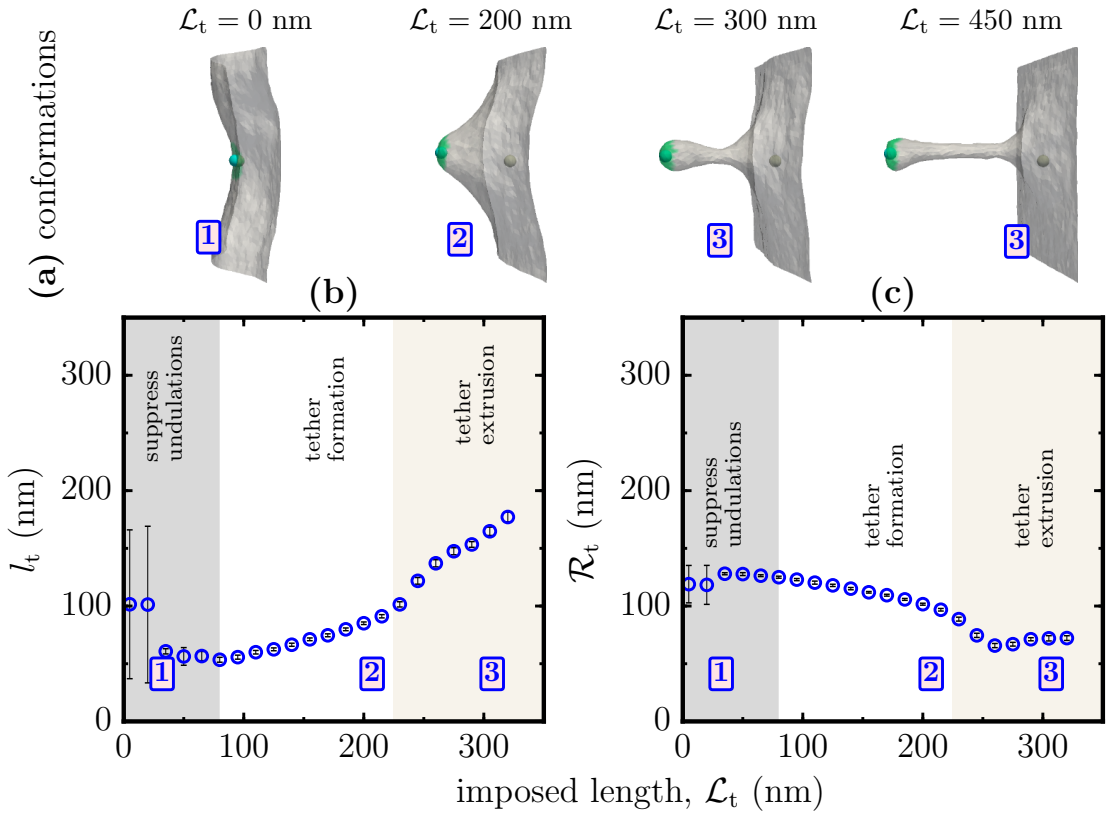

Figure S6. The length and radius of the tether extracted from a membrane with $\kappa = 20\,k_{\rm B}T$ and $\mathcal{A}_{\rm ex} \sim 10\%$ as a function of the imposed tether length $\mathcal{L}_{\rm t}$.

Similarly, in Fig. S7 we show the effect of κ on $l_{\rm t}$ and $\mathcal{R}_{\rm t}$ for membranes with similar excess areas, chosen to be $\mathcal{A}_{\rm ex} \sim 10\%$. The tether pulling data is displayed for $\kappa = 20$, and $160\ k_{\rm B}T$.

As noted in the discussions on Fig.2 in the main manuscript, we find both the systems to exhibit the three distinct scaling regimes previously identified for the tether radius. However, for the membranes with low excess area considered here we find the third regime to occur at a smaller value of $\mathcal{L}_{\rm t}$ compared to that seen for membranes with large excess areas. Similarly, the value of $\mathcal{R}_{\rm t}$ in the final regime is an increasing function of κ, as is evident from Fig. S7.

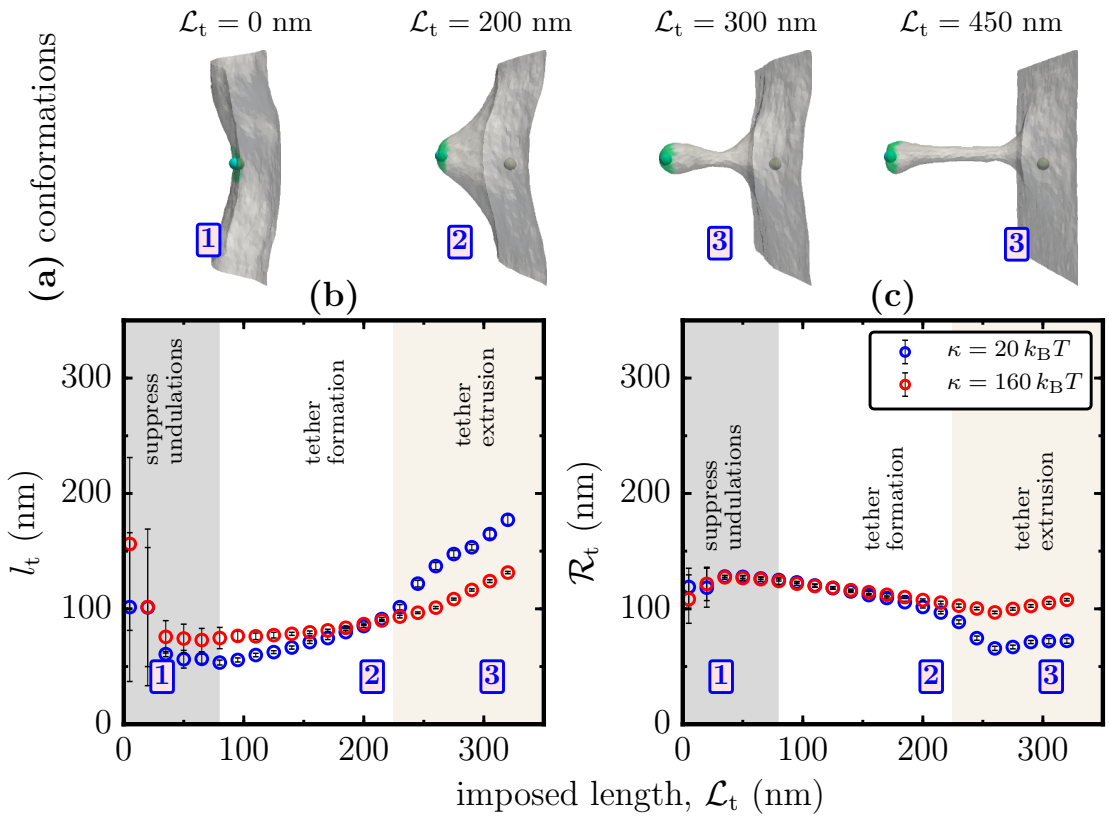

Figure S7. Effect of κ on the length and radius of the extracted tether as a function of the imposed tether length $\mathcal{L}_t$, for membranes with similar excess areas, taken to be $\mathcal{A}_{ex} \sim 10\%$.

S7. Tether pulling experiments

A typical tether pulling experiment proceeds through many stages as illustrated in Fig. S8. In the first stage, the tip of an atomic force microscope (AFM), attached to a cantilever, is indented into the cell surface and held fixed until the tip makes a contact with the cell membrane; these stages are illustrated in Figs. S8(a) and (b). Stage (b) in the experiments is analogous to the initial configurations used in our simulations. After the formation of a stable contact the AFM tip is retracted at a constant velocity until it returns to its undeflected state, as shown in Figs. S8(c) and (d). In the course of retraction the adherence between the tip and the membrane leads to formation of a tether followed by its extrusion and these process are identical to those observed in our simulations and described in Sec.4 of the main manuscript.

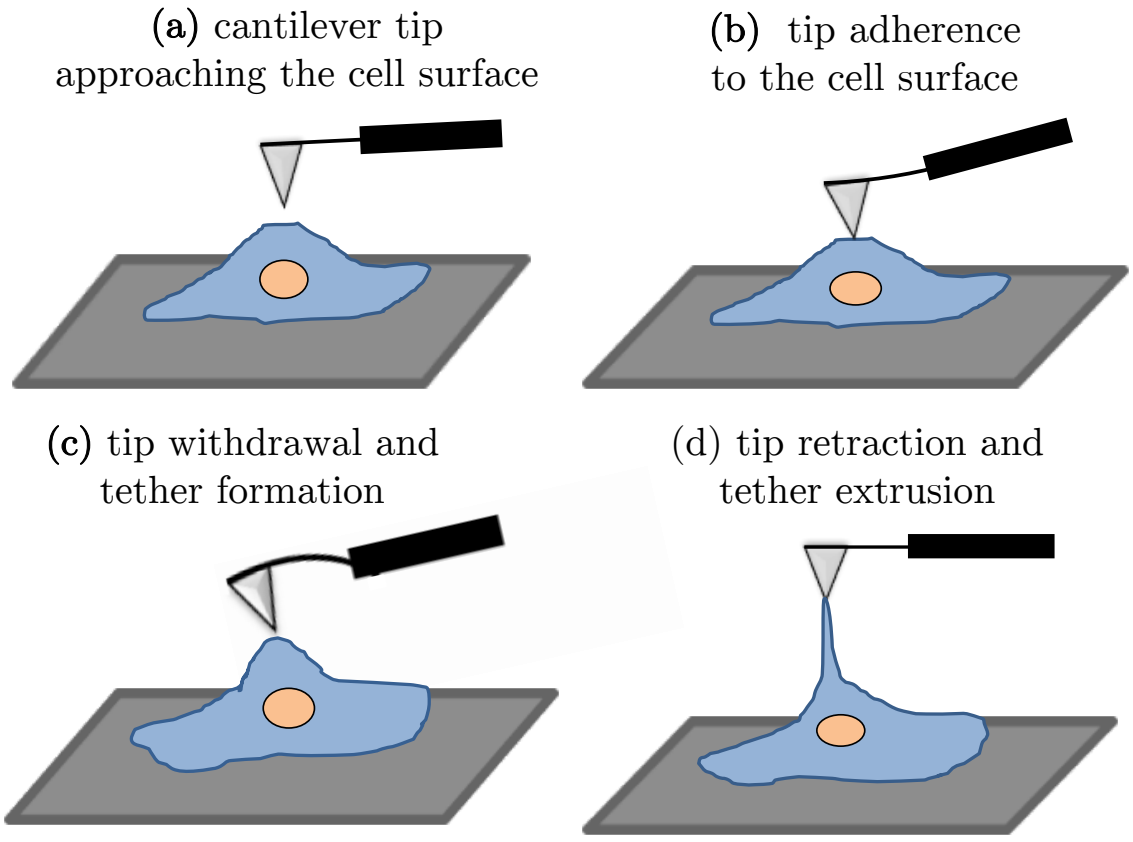

Figure S8. Various stages of a tether pulling experiment.

S8. Comparison of tether characteristics in the constant N-σ-$\mathcal{A}_{\rm patch}$-T and N-σ-τ-T ensembles

The data shown in Fig. S9 corresponds to that shown in Fig.8 in the main manuscript.

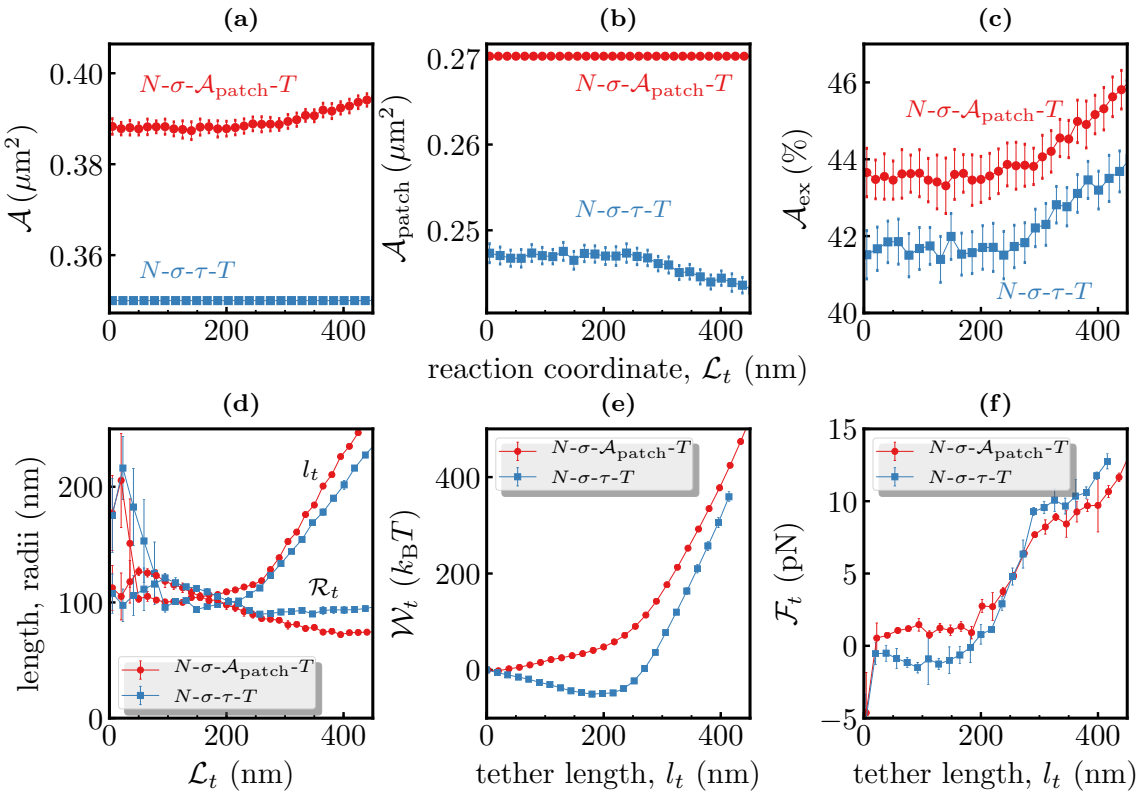

Figure S9. Comparison of tether characteristics in the constant N-σ-τ-T and the constant N-σ-$\mathcal{A}_{\rm patch}$-T ensembles. Panels (a), (b) and (c) show the area ($\mathcal{A}$), projected area ($\mathcal{A}_{\rm patch}$) and excess area ($\mathcal{A}_{\rm ex}$) as a function of the reaction coordinate $\mathcal{L}_{\rm t}$. Panels (d)-(f) are same as that shown in Fig.8 in the main manuscript.

S9. Mechanical properties of the 15 different cells in the CNS

Here we show data from Pontes et. al. [6] for the mechanical properties of 15 different cells in the central nervous system (CNS). The tether force $\mathcal{F}_t$ and radius $\mathcal{R}_t$ for each of these cells (marked C1–C15) satisfies the scaling relation $\mathcal{F}_t\mathcal{R}_t/(2\kappa) = \pi$ and this is shown in Fig. S10(a). The values of κ and σ are shown in Fig. S10(b) and the spread of the data show three characteristic mechanical regimes namely: (i)low κ and low σ, (ii)low κ and high σ, and (iii) high κ and high σ.

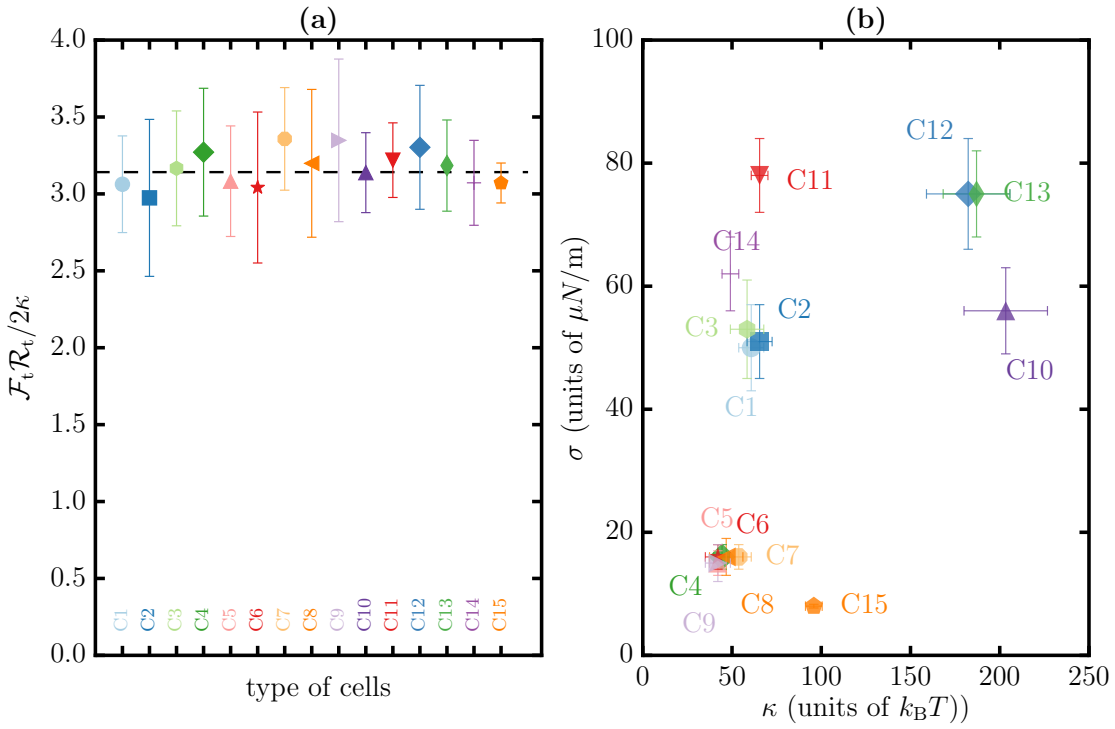

Figure S10. (a) The scaling relation $\mathcal{F}_t\mathcal{R}_t/2\kappa$ and (b) the values of κ and σ for 15 different cells (marked C1–C15) in the CNS. Data from Pontes et. al. [6].

S10. Movie M1

The movie shows the conformations of a tether extracted from a planar membrane as a function of the reaction coordinate $\mathcal{L}_\mathrm{t}$ – data shown for a membrane with $\mathcal{L}_\mathrm{patch} = 510$ nm, $\kappa = 40\ k_\mathrm{B}T$, and $\mathcal{A}_\mathrm{ex} \sim 40\%$ in the constant N-σ-$\mathcal{A}_\mathrm{patch}$-$T$ ensemble. The histogram shown alongside corresponds to the distribution of the mean curvature of the membrane surface

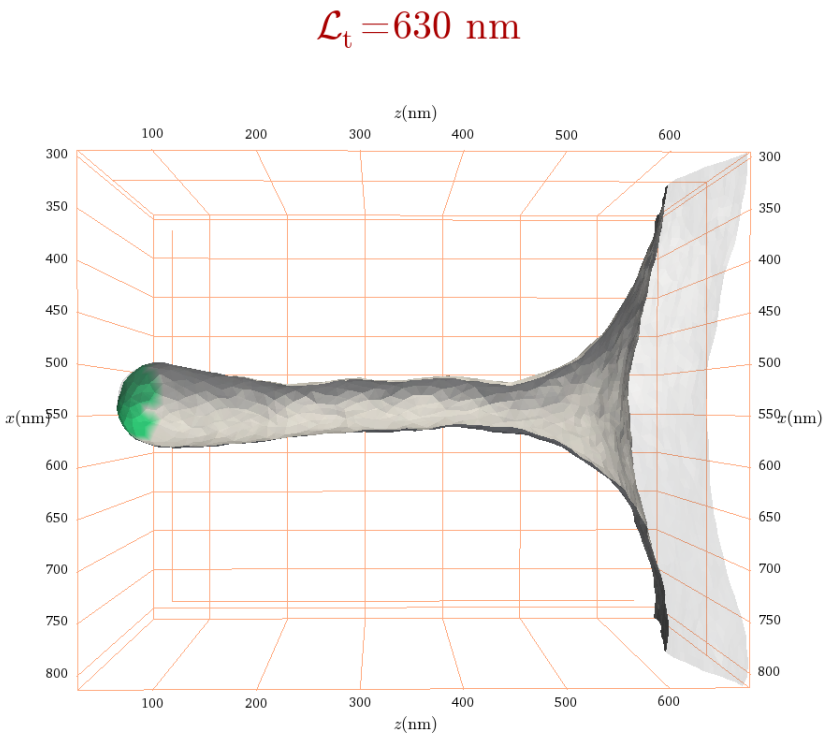

Figure S11. Movie showing the evolution of tether as a function of the reaction coordinate $\mathcal{L}_\mathrm{t}$.

S11. Generating membrane patches with different excess areas

In all our simulations we work with a triangulated surface containing N^2 vertices. These surfaces were generated by triangulating an initial $N \times N$ square grid, with a grid spacing a. This sets the patch size to be $\mathcal{L}_{\rm patch} = Na$ and the projected area to be $\mathcal{A}_{\rm patch} = {\mathcal{L}_{\rm patch}}^2$. The projected area of the membrane patch can be altered either by changing N or by changing a. In all our studies, we take $N = 50$ and choose a to set the desired value of $\mathcal{A}_{\rm patch}$. The square grid is then equilibrated using the DTMC techniques to obtain a curved membrane patch with curvilinear area $\mathcal{A}$. The equilibrated membrane is then used as the starting configuration in our tether pulling simulations. We impose self avoidance in triangulated surface simulations by constraining the length of the link connecting two neighboring vertices. We denote this length by b and its instantaneous value for any link is taken to be in the range $b_{\rm min} < b < \sqrt{3}b_{\rm min}$ [1–3].

(i) **Constant N-σ-τ-T systems:** In this ensemble, both the curvilinear and projected areas, $\mathcal{A}$ and $\mathcal{A}_{\rm patch}$, respectively, are allowed to fluctuate and their fluctuations are governed the surface and frame tensions, σ and τ, respectively. In addition to these, the curvilinear area is coupled to the incompressibility constraint $\mathcal{K}_A(\mathcal{A} - \mathcal{A}_0)^2/2$, as described in Equation 1 of the main manuscript. Since we take $\sigma = 0$ in all our calculations, we set the desired value of $\mathcal{A}$ by tuning $\mathcal{A}_0$. The corresponding value of the projected area is determined by the value of frame tension τ, as is shown in Fig. 1 of the main manuscript and also in Fig. S2.

(ii) **Constant N-σ-$\mathcal{A}_{\rm patch}$-T ensemble:** In this ensemble, we fix the projected area and only allow the curvilinear area to fluctuate. It should be noted that the incompressibility term described above is not used here. Since we perform all our simulations with $\sigma = 0$, we use the self avoidance condition to generate membrane patches with fixed projected but varying curvilinear areas. For a given value of $\mathcal{A}_{\rm patch}$, we generate membranes patches with different curvilinear areas $\mathcal{A}$ by suitably choosing the minimum bondlength $b_{\rm min}$. We adopt this route since it is computationally expensive to change membrane area while holding $\mathcal{A}_{\rm patch}$ to be fixed. This approach effectively modulates the membrane tension and hence yield patches with varying areas, as is shown in our earlier work [7]. Some sample parameters to generate excess area for the constant N-σ-$\mathcal{A}_{\rm patch}$-T ensemble is given in Table 1.

$\mathcal{A}_{\rm ex}$	N	a (nm)	$b_{\rm min}$ (nm)
40%	50	10.0	9.75
20%	50	10.0	9.0
10%	50	10.0	8.5
5%	50	10.0	8.25

Table 1. Minimum bondlength $b_{\rm min}$ used to generate membrane patches of different excess areas in the constant N-σ-$\mathcal{A}_{\rm patch}$-T simulations.

References

[1] D M Kroll and G Gompper. The conformation of fluid membranes: Monte Carlo simulations. *Science*, 1992.

[2] A Baumgärtner and W Renz. Crumpled self-avoiding tethered surfaces. *Euro. Phys. Lett.*, 1992.

[3] N Ramakrishnan, P B Sunil Kumar, and John H Ipsen. Monte Carlo simulations of fluid vesicles with in-plane orientational ordering. *Phys. Rev. E*, 2010.

[4] Nicholas Metropolis, Arianna W Rosenbluth, Marshall N Rosenbluth, Augusta H Teller, and Edward Teller. Equation of State Calculations by Fast Computing Machines. *J. Chem. Phys.*, 1953.

[5] U Seifert. Configurations of fluid membranes and vesicles. *Advances in Physics*, 1997.

[6] Bruno Pontes, Yareni Ayala, Anna Carolina C Fonseca, Luciana F Romão, Racκele F Amaral, Leonardo T Salgado, Flavia R Lima, Marcos Farina, Nathan B Viana, Vivaldo Moura-Neto, and H Moysés Nussenzveig. Membrane Elastic Properties and Cell Function. *PLoS ONE*, 2013.

[7] Richard W Tourdot, N Ramakrishnan, and R Radhakrishnan. Defining the free-energy landscape of curvature-inducing proteins on membrane bilayers. *Phys. Rev. E*, 2014.